NASA/TP—2017–219635

The Influence of G_I and G_{II} on the Compression After Impact Strength of Carbon Fiber/Epoxy Laminates and Sandwich Structure

A.T. Nettles and L.L. Scharber
Marshall Space Flight Center, Huntsville, Alabama

July 2017

The NASA STI Program…in Profile

Since its founding, NASA has been dedicated to the advancement of aeronautics and space science. The NASA Scientific and Technical Information (STI) Program Office plays a key part in helping NASA maintain this important role.

The NASA STI Program Office is operated by Langley Research Center, the lead center for NASA's scientific and technical information. The NASA STI Program Office provides access to the NASA STI Database, the largest collection of aeronautical and space science STI in the world. The Program Office is also NASA's institutional mechanism for disseminating the results of its research and development activities. These results are published by NASA in the NASA STI Report Series, which includes the following report types:

- TECHNICAL PUBLICATION. Reports of completed research or a major significant phase of research that present the results of NASA programs and include extensive data or theoretical analysis. Includes compilations of significant scientific and technical data and information deemed to be of continuing reference value. NASA's counterpart of peer-reviewed formal professional papers but has less stringent limitations on manuscript length and extent of graphic presentations.

- TECHNICAL MEMORANDUM. Scientific and technical findings that are preliminary or of specialized interest, e.g., quick release reports, working papers, and bibliographies that contain minimal annotation. Does not contain extensive analysis.

- CONTRACTOR REPORT. Scientific and technical findings by NASA-sponsored contractors and grantees.

- CONFERENCE PUBLICATION. Collected papers from scientific and technical conferences, symposia, seminars, or other meetings sponsored or cosponsored by NASA.

- SPECIAL PUBLICATION. Scientific, technical, or historical information from NASA programs, projects, and mission, often concerned with subjects having substantial public interest.

- TECHNICAL TRANSLATION. English-language translations of foreign scientific and technical material pertinent to NASA's mission.

Specialized services that complement the STI Program Office's diverse offerings include creating custom thesauri, building customized databases, organizing and publishing research results…even providing videos.

For more information about the NASA STI Program Office, see the following:

- Access the NASA STI program home page at <http://www.sti.nasa.gov>

- E-mail your question via the Internet to <help@sti.nasa.gov>

- Phone the NASA STI Help Desk at 757–864–9658

- Write to:
  NASA STI Information Desk
  Mail Stop 148
  NASA Langley Research Center
  Hampton, VA 23681–2199, USA

NASA/TP—2017–219635

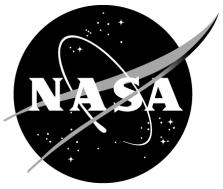

The Influence of G_I and G_{II} on the Compression After Impact Strength of Carbon Fiber/Epoxy Laminates and Sandwich Structure

A.T. Nettles and L.L. Scharber
Marshall Space Flight Center, Huntsville, Alabama

National Aeronautics and
Space Administration

Marshall Space Flight Center • Huntsville, Alabama 35812

July 2017

Available from:

NASA STI Information Desk
Mail Stop 148
NASA Langley Research Center
Hampton, VA 23681–2199, USA
757–864–9658

This report is also available in electronic form at
<http://www.sti.nasa.gov>

TABLE OF CONTENTS

LIST OF FIGURES

LIST OF FIGURES (Continued)

LIST OF TABLES

LIST OF ACRONYMS

BVID	barely visible impact damage
CAI	compression after impact
DCB	double cantilever beam
DIC	digital image correlation
ENF	end notched flexure
FOD	foreign object debris
NDE	nondestructive evaluation
OHC	open-hole compression

TECHNICAL PUBLICATION

THE INFLUENCE OF G_I AND G_{II} ON THE COMPRESSION AFTER IMPACT STRENGTH OF CARBON FIBER/EPOXY LAMINATES AND SANDWICH STRUCTURE

1. INTRODUCTION

Since compression after impact (CAI) strength is often a major design driver of components made with carbon fiber/epoxy matrix laminates, understanding the failure process would be beneficial to help develop more damage-tolerant laminates and to help with the analytical modeling of the compressive load-carrying capabilities of impact damaged laminates. In an effort to examine damage growth during CAI tests to aid in this understanding of the failure process, the author has performed many experiments in which CAI tests were stopped at approximately 95%–99% of the expected failure load and the specimens subsequently examined using nondestructive evaluation (NDE) in an attempt to observe delamination growth. These specimens were then dissected to ensure that any delamination growth that the NDE might have missed was not present. Upon discovering no observable delamination growth, the author then employed high-speed digital image correlation (DIC), in which the growing delamination near failure would be captured by examining the of out-of-plane displacement (blistering) enlargement. Even with this method, in which sublaminate buckling (blistering) appeared evident, the buckled zone (blister size) was never bigger than the original damage area; thus, no damage growth was found, even on lay-ups that should have facilitated delamination growth. It should be noted that within milliseconds of failure, damage extension across the specimen width was detected, but whether this was delamination growth or kink band formation and propagation could not be determined. All CAI failures were catastrophic, and the only tests that resulted in any kind of progressive damage growth well before failure consisted of fiber microbuckling (kink band) growth emanating from the edge of the damage area if 0º plies were clumped on the outside of the specimen. These CAI specimens were sandwich structure, and the DIC data indicated that the sublaminate buckling was inward towards the core; thus, it was deduced that the core may have suppressed the delamination growth. However, these results brought into question the mechanism of failure of most CAI tests, since delamination growth appears to be the most popular model.[1–29]

Experimental evidence of delamination growth during a CAI test is rather sparse, but has been noted to various extents.[1,3,9,18,24,28] To the author's knowledge, there have been no claims of finding delamination growth along the length of a specimen during experiments. The growth, if observed, has always been perpendicular to the loading direction.

In order to more closely interrogate the sequence and mode of failure of carbon/epoxy laminates during a CAI test, the basic mechanisms of the test can be isolated and some simple observations made. These observations are based on the assumption that CAI strength is driven by both

mode I (opening) and mode II (sliding) interlaminar strength between plies. It is also assumed that the damage resistance component is more mode II dominant and that the residual compression strength testing component is more mode I dominated. This is sketched for clarity in figure 1 (mode II governing damage formation) and figure 2 (mode I governing residual compression strength). This is a key assumption—and a rather simplistic one—since some combination of mode I, mode II, and mode III fracture is likely present in all phases of the CAI test.

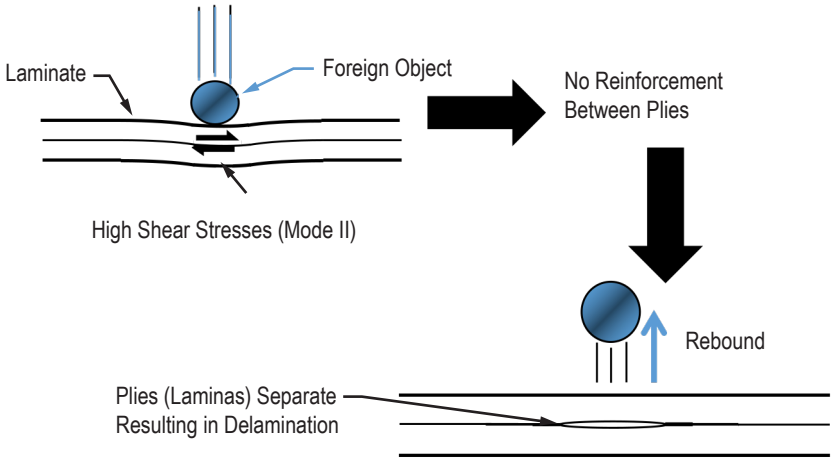

Figure 1. Schematic of the damage resistance phase of the CAI test.

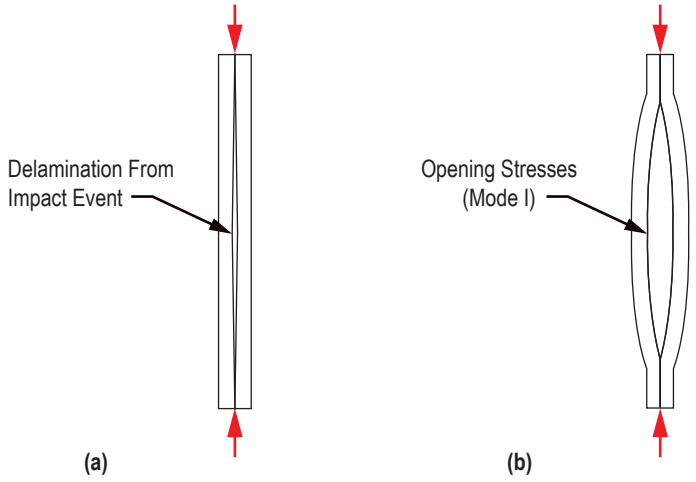

Figure 2. Schematic of the residual strength phase of the CAI test: (a) Start of compression test and (b) delamination growth during test.

One observation that can be made to determine if delamination growth is a mechanism governing CAI strength values is by first varying a parameter that is expected to affect delamination growth, and then noting the differences in experimental results of the CAI tests. This can be done without having to actually witness the delamination growth which, if it does occur, is difficult to detect since the failure is usually catastrophic. Since it is assumed that delamination growth during in-plane loading is mainly (not totally) an opening or mode I type separation of plies (as sketched in fig. 2), then having laminates with varying fracture toughness (G_I) values should produce different CAI strength results for a given damage state. This concept is sketched on the two plots in figure 3 as a visual representation. If two fiber/resin systems have equal mode II toughness values, but one has a higher mode I toughness value, then the damage size is expected to be about the same for both for any given impact energy. Subsequently, upon compressive loading, the system with the higher mode I toughness is assumed to resist damage growth more—resulting in a higher CAI strength value—compared to the system with the lower mode I toughness value.

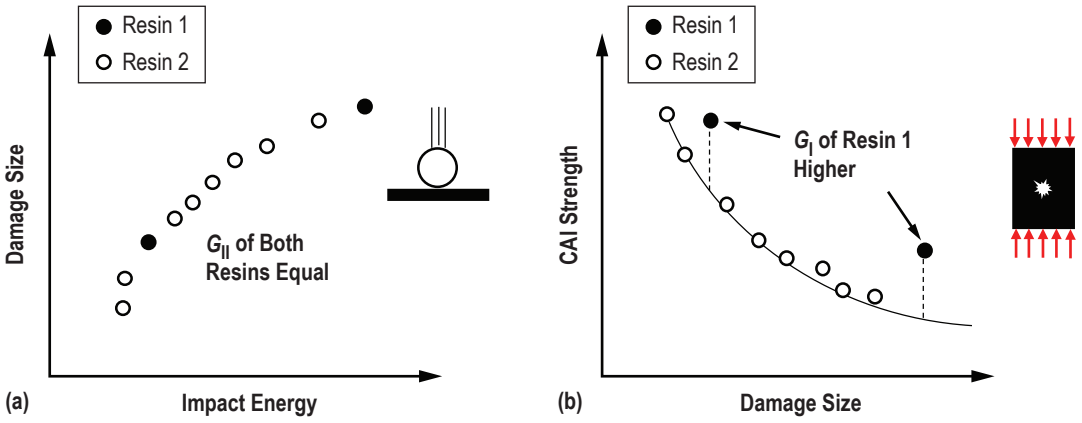

Figure 3. Schematic of increased CAI strength due to increased mode I toughness for two fiber/resin systems: (a) Formation of damage—similar G_{II} values should give similar damage sizes and (b) higher G_I value should give higher CAI strength values for a given damage size.

In three studies that measured CAI strength and both mode I and mode II toughness modes,[30–32] there was found to be an approximate linear correlation between CAI strength and mode II fracture toughness, but there was no discernable correlation between mode I toughness and CAI strength. In these studies, it was noted that the damage area formed due to the impact event was much smaller for specimens with a higher mode II toughness and this caused most of the CAI strength improvement.

This dependence of CAI strength on mode II toughness (smaller damage size) rather than mode I toughness (resistance to delamination growth) is evidenced by CAI strength versus impact energy plots showing distinct differences between toughened and untoughened systems; but when plotted as CAI strength versus damage size, the CAI strength curves are more similar for both toughened and untoughened systems.[33–39] This concept is sketched for clarity in figure 4. These results

indicate that the CAI strength of laminates is not heavily affected by delamination growth during in-plane loading since the tougher laminates would be expected to have a notably higher CAI strength for a given damage size considering that delamination growth should be suppressed.

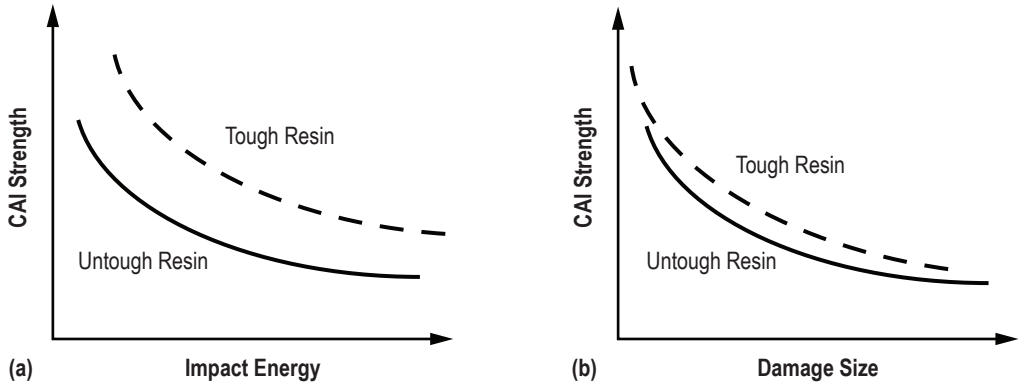

Figure 4. Schematic of the residual compressive strength of laminates: (a) As a function of impact energy and (b) as a function of damage size.

Since CAI strength is related to damage size in much the same way as open-hole compression (OHC) strength is related to hole size,[40–42] a fiber microbuckling (kink band) mode of failure similar to holes has been suggested for the failure mechanism of a CAI test. The kink band formation-equivalent hole model has been used by others to assess CAI strength of laminates.[43–51] In this model, for a given damage size, the remaining compression strength of an impact-damaged laminate should be relatively independent of changes in G_I and G_{II} since failure is by 0º fiber kink band formation and propagation, not delamination growth. An examination of vendor data reveals that OHC strength is fairly independent of resin toughness and most published values are in the 310–345 MPa range (for IM7 carbon fiber-based quasi-isotropic laminates) despite different toughness resins, thus kink band formation (the mechanism of failure for OHC laminates) does not appear to be dependent on G_I or G_{II}.

If the opening mode (G_I toughness) was significant in CAI tests, then through thickness reinforced laminates—such as those that are stitched—would derive the majority of their CAI strength improvement as a result of increased delamination growth resistance for a given damage size, not from a reduction in damage size during the impact event. The results in the open literature on stitched laminates tend to show improvement in CAI strength due to the stitching, causing a smaller damage area, but in at least one case, there is evidence of an even greater CAI strength improvement other than what would be expected—just to a smaller damage area;[52] i.e., the behavior in figure 3(b) was seen for one specimen.

Recent work[53] has suggested a model of CAI failure whereby delamination growth within the already existing damage zone (undamaged cone of material directly under the impact site) is a contributor to the CAI strength of laminates. It specifically mentions the two competing failure

mechanisms of load-bearing fiber microbuckling and delamination growth, with this model having aspects of both. This study used interrupted testing (stopping the test just before failure) with ex situ microfocus computed tomography to examine the state of damage so that the specimen could be reloaded for further testing. To the author's knowledge, the only other CAI testing programs in which interrupted tests showed any damage evolution are in references 49 and 50. In these studies, kink band formation was evident and quantified. Some delamination growth was noted from an embedded defect (as opposed to impact damage) in interrupted testing in references 9 and 29; however, this study is concerned with damage due to impact, not foreign object debris (FOD) between plies.

In order to help determine the relative mode I and mode II toughness contributions to CAI strength, a systematic series of tests was performed at NASA Marshall Space Flight Center in which the CAI strength of IM7 carbon fiber composites in a variety of epoxy resins of various toughness values was assessed. The toughness values of the fiber/resin systems were established by the double cantilever beam (DCB) test and the end notched flexure (ENF) test. In addition, OHC testing was also performed to see if resin toughness values had any effect on this strength value, since modeling impact damage as an equivalent hole has been suggested.[43–50] By having all specimen preparation and testing of the various fiber/epoxy systems performed by the same personnel at the same laboratory, variations due to specimen preparation and testing are thought to be minimized and a more representative database than those in references 30 through 32, which had only a few resin systems or data from many different studies combined. Since much of the author's work is with sandwich structure, four of the seven carbon fiber/resin systems used were tested as face sheets of honeycomb core sandwich structure to assess any differences that this may or may not cause.

2. MATERIAL

All of the laminates and sandwich structure tested in this study had unidirectional IM7 fiber as the reinforcement. This was done so that the resins, and not the fibers, could be compared. A total of seven IM7/epoxy systems were used. The ultimate goal of having a variety of resins was to obtain a wide range of mode I and mode II toughness values.

Since some of the prepregs used were out of shelf life, or during the processing, the manufacturer's recommended cure cycle was not strictly adhered to, the trade names of the matrix resins will be replaced by identification numbers. The identification numbers were chosen in order of measured G_{II} values, with the highest G_{II} being called resin 1, the next highest resin 2, etc.

A list of the laminates used in this study are given in table 1, along with the nominal ply thickness and fiber volume fraction of each laminate. All laminates were void free. The fiber volume fraction was calculated using digital photo microscopy.

Table 1. Fiber/resin systems used in this study.

Resin Identifier	Nominal Cured Ply Thickness (mm)	V_f (%)
1	0.137	56
2	0.135	58
3	0.135	58
4	0.119	61
5	0.137	57
6	0.137	57
7	0.142	54

The CAI and OHC laminates consisted of a 32-ply lay-up with the stacking sequence $[45,0,–45,90]_{4S}$. Sections of the laminates produced were checked for void content and fiber volume fraction, and results showed good repeatability for any given fiber/resin system. The sandwich structure tested for CAI strength consisted of 16-ply quasi-isotropic lay-ups with a stacking sequence of $[45,0,–45,90]_{2S}$. The face sheets were cured on a flat caul plate before bonding to the glass/phenolic honeycomb core, thus no fiber waviness was present as is typical of a co-cured honeycomb sandwich structure. The glass/phenolic core had a nominal density of 88 kg/m^3.

3. EXPERIMENTAL

Some of the details of the experimental tests are given in this section. The most important aspect of the tests conducted in this program was to be consistent between all fiber/resin systems. In order to achieve this, all specimens were prepared and tested in an identical manner by the same personnel, so any biases would be minimized and a better comparison of material response could be measured. Thus, sufficient detail of each test will be given so the reader will have a better understanding of the resulting toughness and strength values presented.

3.1 End Notch Flex

Approximate values for the mode II toughness of the various fiber/resin systems was established using the ENF test, as outlined in reference 54. A schematic of this test is shown in figure 5. Initially, the compliance calibration method was used; however, the areas method was eventually favored, since similar results in mode II fracture toughness values were being obtained by this method. Since the relative toughness between fiber/resin systems in this study was more important than the actual strain energy release rate values (since design data were not being generated), this was deemed acceptable for comparison purposes of values within this study.

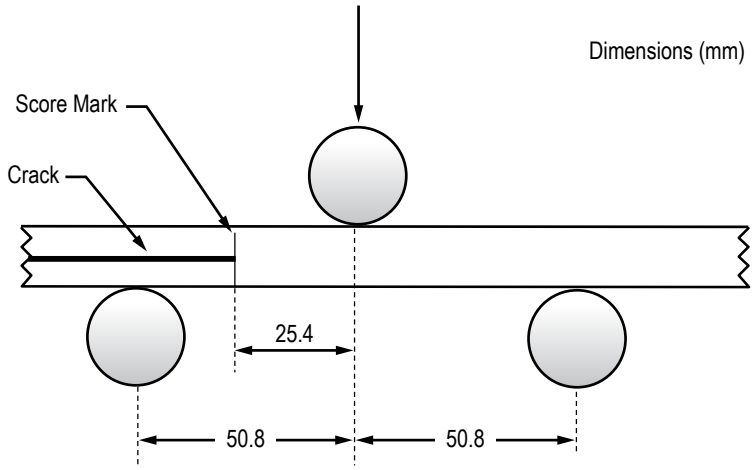

Figure 5. Schematic of the ENF test used in this study.

The ENF specimens were manufactured as 24-ply unidirectional laminates with a teflon insert at the midplane on one end of the specimens. A precrack was made from the end of this insert by placing the specimen in a three-point-bend fixture and loading until a crack grew from the end of the teflon insert to produce a ‘natural’ crack front. The end of this natural crack was marked on the specimen by observation under a microscope and cutting a score mark at the end of the crack using a razor blade. Afterwards, the

specimen was placed back in the three-point-bend fixture and loaded until another increment of crack growth occurred. The specimen was then removed, and the new end of the crack was noted on each side and marked on the specimen. To obtain a value for crack length, these length measurements on both sides were averaged. This distance was multiplied by the specimen width to obtain the amount of new surface area formed. The energy required to create this surface area was calculated from the area under the load-displacement curve, as shown in figure 6. The mode II fracture toughness, denoted by G_{II}, was calculated by dividing the energy by the surface area created. This process was repeated down the length of the specimen until the crack reached within 7 cm of the end of the specimen. Each specimen could yield three or four measurements before the crack reached the end of the specimen. At least six specimens were tested for each fiber/resin system.

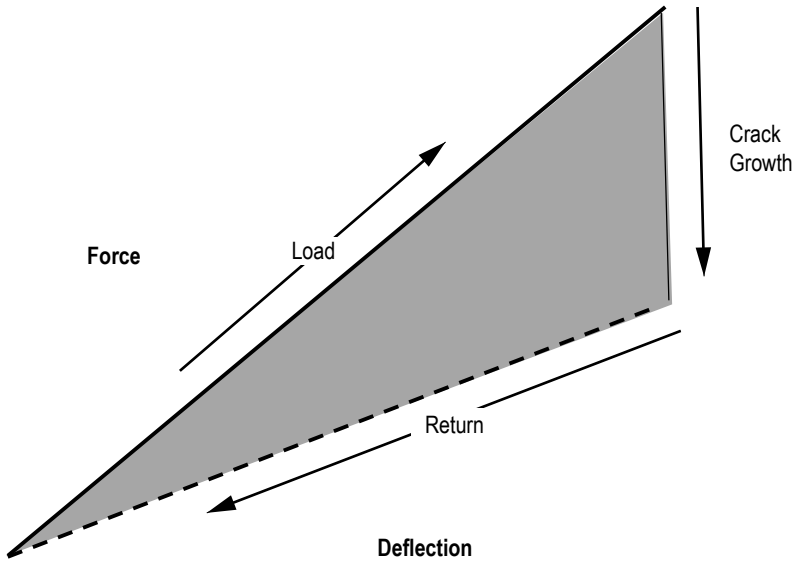

Figure 6. Schematic of load-displacement curve for ENF test with the energy to create the new surface area noted by the shaded region.

3.2 Double Cantilever Beam

Approximate values for the mode I toughness of the various fiber/resin systems were established using the DCB test as outlined in reference 55. A schematic of this test is shown in figure 7. Initially, the modified beam theory was used; however, the areas method was eventually favored since similar results in mode I fracture toughness values were being obtained by this method. Since the relative toughness between fiber/resin systems in this study was more important than the actual strain energy release rate values (considering that design data were not being generated), this was deemed acceptable for comparison purposes within this study.

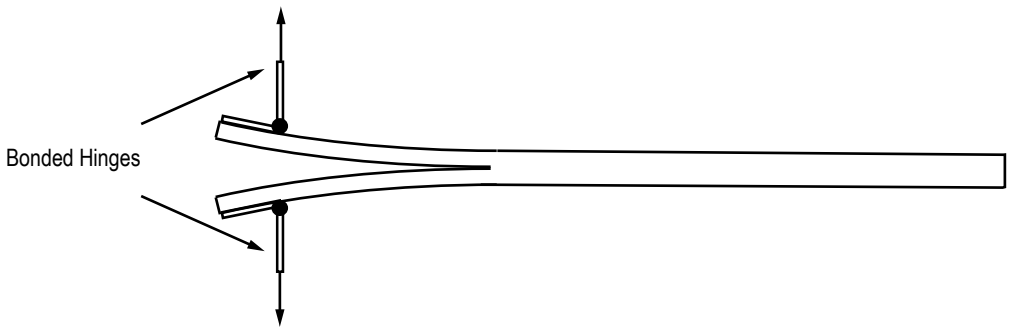

Figure 7. Schematic of the DCB test.

The DCB specimens were manufactured as 30-ply unidirectional laminates with a teflon insert embedded in the midplane at one end to start the crack growth process. Once the initial crack was started from the end of the teflon insert (to produce a natural crack front), the specimens were removed and the end of the natural crack tip was noted on each side of the specimen. The specimen was then reloaded, and the test was performed continuously until the crack had grown approximately 10 cm. The specimen was then removed and the new end of the crack was noted on both sides of the specimen. These two lengths were averaged to obtain the overall length of the new crack formed. This length was multiplied by the specimen width to obtain the amount of surface area created during the test. The energy needed to grow the crack was calculated from the load-displacement curve, as shown schematically in figure 8. The G_I value was calculated by dividing this energy by the surface area created. At least five specimens from each fiber/resin system were tested.

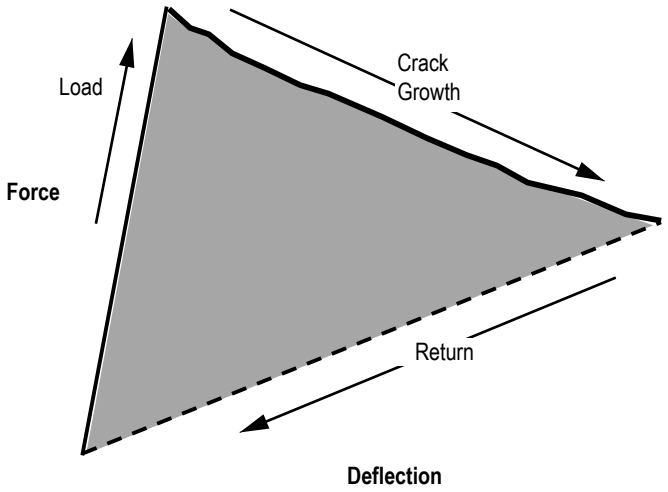

Figure 8. Schematic of load-displacement curve for DCB test with the energy to create the new surface area noted by the shaded region.

3.3 Open-Hole Compression

Values for the OHC strength of the various fiber/resin systems was established using ASTM D6484.[56] Specimens consisted of 32-ply quasi-isotropic laminates with a stacking sequence of $[45/0/–45/90]_{4S}$. The results were normalized to 60% fiber volume fraction ($V_f = 60\%$).

3.4 Compression After Impact

3.4.1 Laminates

Values for the CAI strength of the monolithic laminates of the various fiber/resin systems was established using ASTM D-7137.[57] Specimens consisted of 32-ply quasi-isotropic laminates with a stacking sequence of $[45/0/–45/90]_{4S}$. The strain on both faces of the specimen, away from the damage area, was monitored during each compression test to make sure no deviation greater than 10% occurred. The CAI strength results were normalized to 60% fiber volume fraction ($V_f = 60\%$). At least six specimens were tested for each fiber/resin system.

The damage was induced by clamping each specimen over a 6.35-cm-diameter opening and impacting at the center with a 12.7-mm instrumented tup. The laminates were all impacted with about 10.8 J of impact energy, and flash thermography was used to assess the planar extent of damage. This impact energy value was chosen because it produced barely visible impact damage (BVID) on a common toughened 32-ply carbon/epoxy laminate and BVID is typically the impact severity level of most interest. An example of flash thermography indication with the damage width used to assess the severity of damage is given in figure 9.

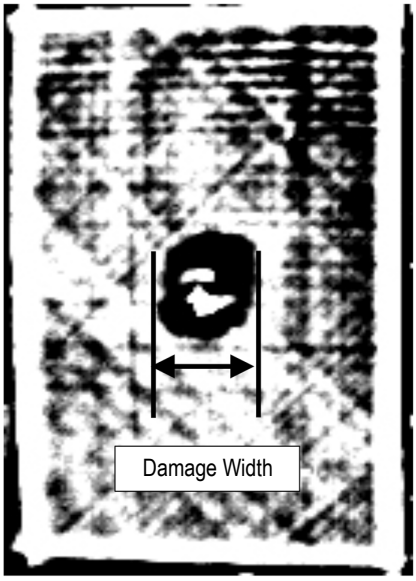

Figure 9. Flash thermography example with damage width noted.

The CAI strength results were normalized to 60% fiber volume fraction ($V_f = 60\%$). At least six specimens were tested for each fiber/resin system.

3.4.2 Sandwich Structure

Values for the CAI strength of sandwich structures with face sheets of the four various fiber/resin systems used to make these structures was established using the methodology detailed in reference 58. Specimens consisted of 16-ply quasi-isotropic laminates that were precured before bonding to the glass/phenolic core, with a stacking sequence of $[45/0/–45/90]_{2S}$. The strain on both faces of the specimen, away from the damage area, was monitored during each compression test to ensure no deviation greater than 10% occurred. The CAI strength results were normalized to 60% fiber volume fraction ($V_f = 60\%$). At least six specimens were tested for each fiber/resin system.

The damage was induced by placing each specimen on a steel plate and impacting at the center with a 12.7-mm instrumented tup. The laminates were all impacted with about 10.8 J of impact energy, and flash thermography was used to assess the planar extent of damage. This value of impact energy was chosen because it produced BVID on a common toughened 16-ply carbon/epoxy sandwich structure, and BVID is typically the impact severity level of most interest. It is assumed to be happenstance that the same value of impact energy was needed to cause BVID in both the 32-ply monolithic laminates and the 16-ply face sheet sandwich structure.

4. RESULTS

The results of the ENF, DCB, OHC, and CAI tests will be summarized in this section.

4.1 End Notch Flex and Double Cantilever Beam

The results of the ENF and DCB tests are shown in table 2.

Table 2. Results of ENF and DCB testing (averages and standard deviations).

Resin System	ENF-G_{II} (J/m^2)	DCB-G_I (J/m^2)
1	2,275 ± 280	420 ± 35
2	1,995 ± 157	507 ± 87
3	1,487 ± 245	455 ± 87
4	1,452 ± 210	665 ± 157
5	1,120 ± 105	350 ± 70
6	857 ± 157	245 ± 35
7	840 ± 70	402 ± 70

In order to examine any relationship between G_I and G_{II}, the average values presented in table 2 are plotted against each other and presented in figure 10. Perhaps a general correlation is noted between G_I and G_{II}, but the correlation has enough variation such that a range of G_I and G_{II} values, not dependent on each other, will be available to isolate each of the toughness values to draw conclusions about the contribution of each to CAI strength.

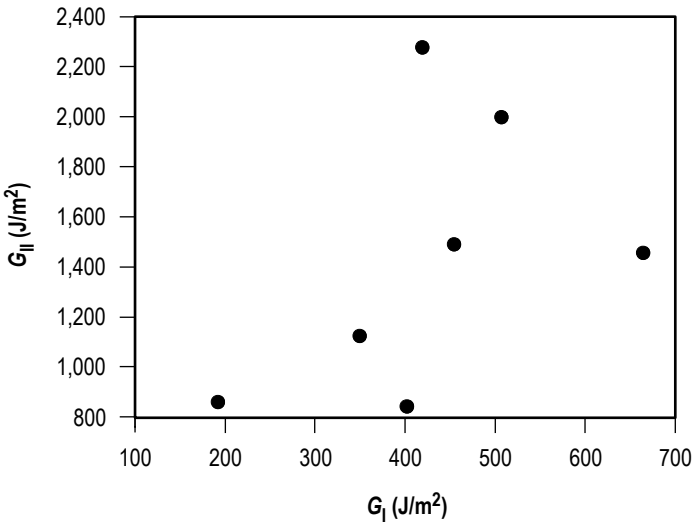

Figure 10. Values of G_{II} versus G_I for the fiber/resin systems tested in this study.

4.2 Open-Hole Compression

The average strength results with standard deviations of the OHC tests are shown in table 3. Each resin system had at least seven repeat tests.

Table 3. Results of the OHC tests.

Resin System	OHC Strength (MPa)
1	346 ± 9
2	326 ± 5
3	324 ± 9
4	331 ± 8
5	339 ± 11
6	No data
7	328 ± 14

These OHC strength results are plotted in figure 11 as a function of each of the mode I and mode II toughness values, as given in table 2. Since the strength results differ so little, no discernable trend between the toughness values and the OHC strengths can be established. All of the values are in the 310–345 MPa range, which are similar to the vendor data as mentioned in the introduction.

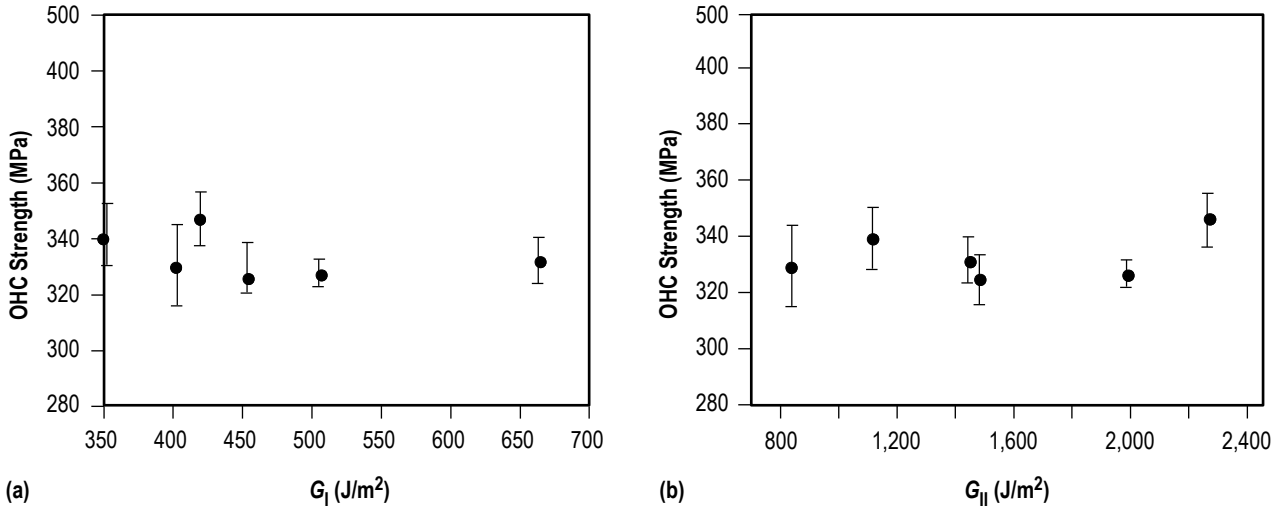

Figure 11. OHC strength values versus (a) G_{I} and (b) G_{II} .

4.3 Laminate Compression After Impact

The average strength results with standard deviations of the 32-ply CAI tests are shown in table 4. Each fiber/resin system had six repeat specimens.

Table 4. Results of the laminate CAI tests.

Resin System	Impact Energy (J)	Damage Width (mm)	CAI Strength (MPa)
1	11 ± 0.5	14.2 ± 1.5	452 ± 30
2	11 ± 0.3	21.1 ± 1	365 ± 26
3	10.8 ± 0.3	25.1 ± 1.3	304 ± 6
4	10.7 ± 0.1	25.4 ± 1.5	303 ± 14
5	10.8 ± 0.1	29.7 ± 1.8	288 ± 22
6	10.6 ± 0.05	31.2 ± 1	279 ± 12
7	11.1 ± 0.1	32.8 ± 1.3	269 ± 6

These CAI strength results are plotted in figure 12 as a function of each of the mode I and mode II toughness values, as given in table 2. The results are similar to those found in references 30–32, in which no distinct relationship between G_{I} and CAI was found and a direct relation between G_{II} and CAI appears to be present. The relationship between G_{II} and CAI does not appear linear, especially at the higher values of G_{II}.

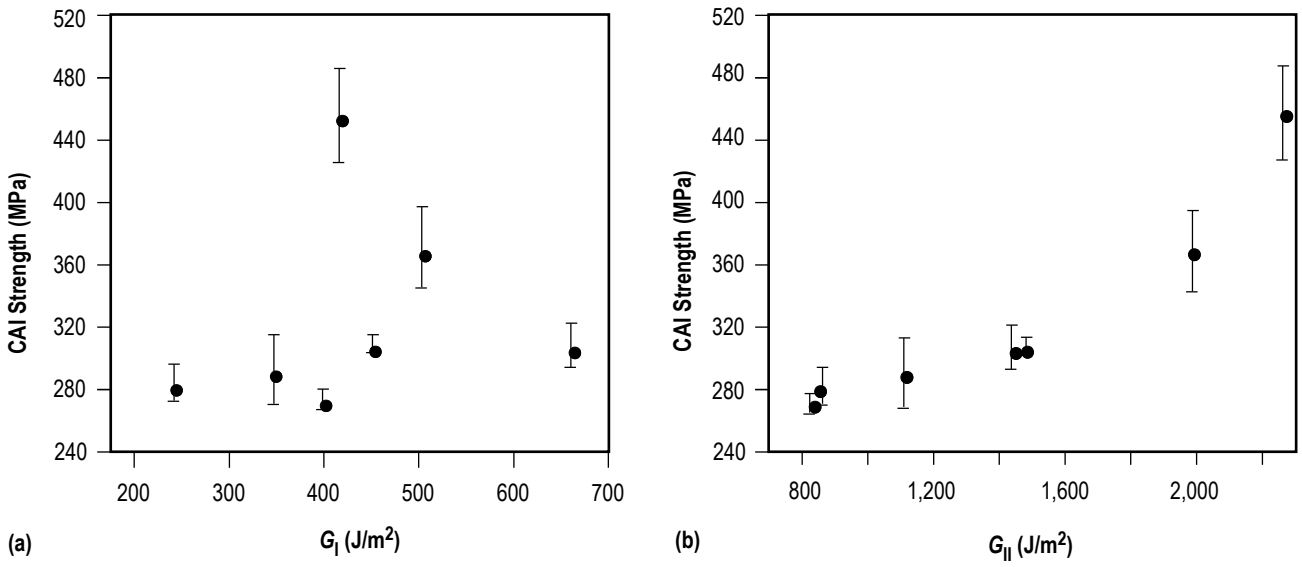

Figure 12. CAI strength values versus (a) G_I and (b) G_{II} for monolithic 32-ply laminates.

4.4 Sandwich Structure Compression After Impact

The strength results with standard deviations of the 16-ply CAI tests on sandwich structure are shown in table 5. Each fiber/resin system had six repeat specimens.

Table 5. Results of the sandwich structure CAI tests.

Resin System	Impact Energy (J)	Damage Width (mm)	CAI Strength (MPa)
1	N/A	N/A	N/A
2	10.7 ± 0.04	27.4 ± 1	293 ± 14
3	11 ± 0.11	30 ± 0.8	265 ± 15
4	N/A	N/A	N/A
5	10.7 ± 0.23	36.3 ± 2	238 ± 9
6	N/A	N/A	N/A
7	10.6 ± 0.68	39.9 ± 1	235 ± 14

These CAI strength results are plotted in figure 13 as a function of each of the mode I and mode II toughness values, as given in table 2. The results are somewhat similar to those found for the 32-ply monolithic laminates, in which a lesser relationship between G_I and CAI was found compared to the relation between G_{II} and CAI, although only one type of specimen did not follow a trend for the G_I versus CAI data.

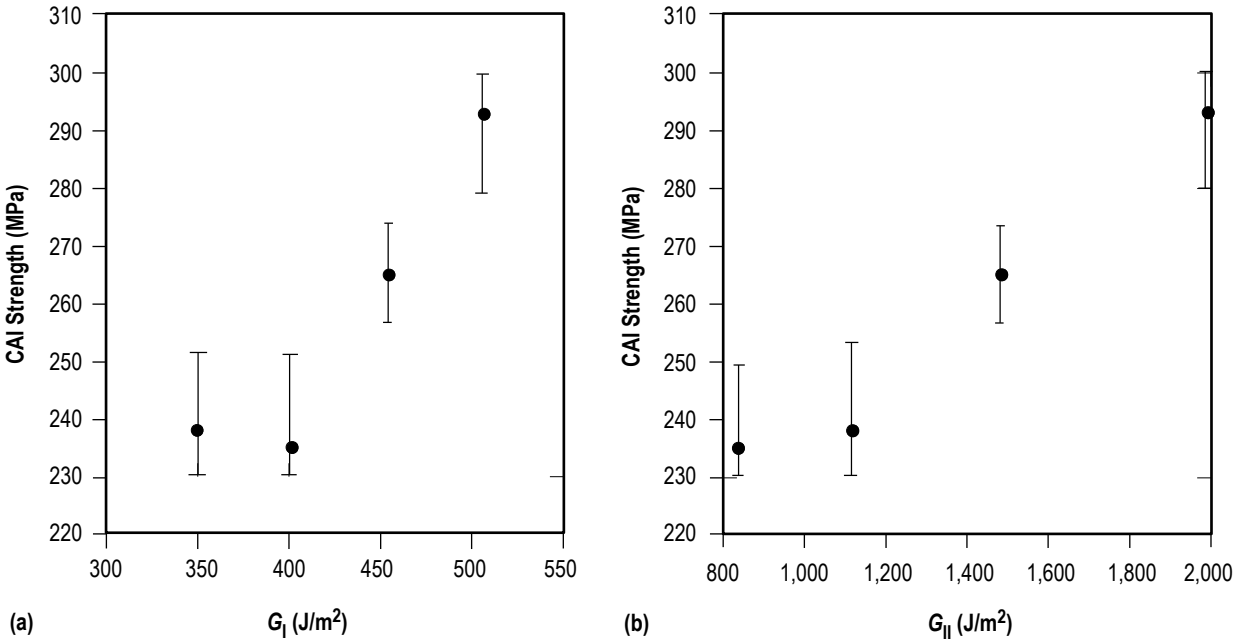

Figure 13. CAI strength values versus (a) G_{I} and (b) G_{II} for sandwich structure.

5. DISCUSSION

Open-hole compression strength does appear to be independent of G_I and G_{II}; thus, kink band formation is assumed to be independent of these toughness values also. As a check that the OHC specimens were indeed failing by kink band formation and propagation, a few OHC test specimens where taken to near failure loads, and then removed from the load frame and cut and polished at the zone shown in figure 14. The accompanying photomicrograph shows kink band formation in the load-bearing 0° plies.

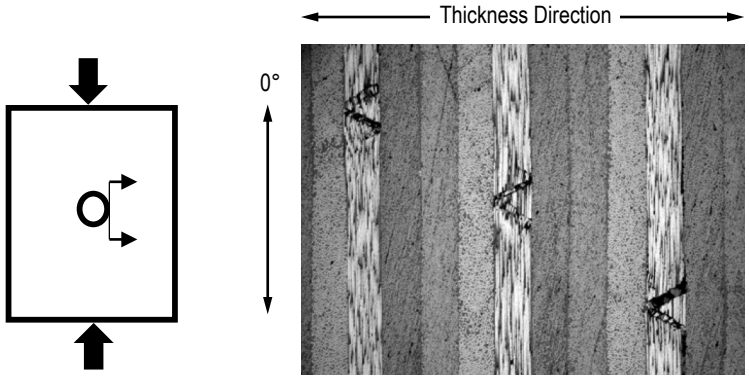

Figure 14. Photomicrograph of 0º fiber kink bands (× 50) from an OHC specimen taken to near expected failure load.

For the 32-ply monolithic laminates, the CAI strength values appear to be independent of the measured G_I values and directly dependent on G_{II} values, as shown in figure 12(b), with higher G_{II} values, giving a higher CAI strength. Since the higher mode I values have no noticeable effect on CAI strength, the indication is that mode I delamination growth during the in-plane compressive loading does not occur, or if it does, it has no effect on the ultimate CAI strength.

For the 16-ply face sheet sandwich structure, the results are less conclusive about the nonrelationship between G_I and CAI strength, although only four of the resin systems were tested. As with the 32-ply monolithic laminates, the G_{II} versus CAI results see a distinctive trend, with higher G_{II} values giving higher CAI strength values.

Figure 15 is a plot of CAI strength versus damage size for all the resin systems, with an exponential best fit curve applied. This type of best fit curve has been shown to characterize CAI strength versus damage size data well.[58] If the mode I toughness values (noted next to each data point) had any effect on the CAI failure mechanism, these data would not fit the curve so well. The laminates with the higher G_I values should have strengths above the best fit curve, as shown schematically in figure 3(b). Conversely, the data with low G_I values would be expected to fall below the best fit curve, but neither is the case. Either

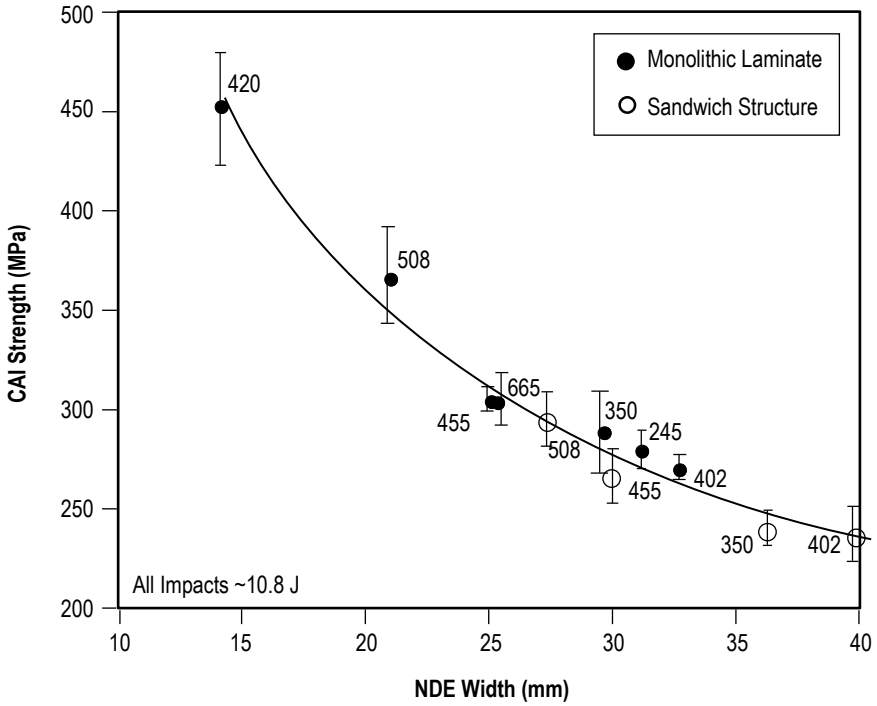

Figure 15. CAI strength versus damage width. G_I values in (J/m^2) listed next to each data point for all seven fiber/resin systems tested.

delamination growth of the mode I type is not occurring during the compressive loading phase, or if it does, the damage growth due to opening-type delamination growth as measured by the DCB test is not responsible for the ultimate compressive failure.

Figure 15 indicates that CAI strength is only dependent on the size of damage that is incurred during the impact event for any given impact energy. If this is true, the damage size should be directly related to G_{II} for a given impact energy level and show no dependence on G_I, based on the assumptions made in figure 1. As a check, the damage sizes incurred are plotted versus G_I and G_{II} in figure 16, and a relationship between G_{II} and damage size is seen to be present. This is not unexpected, as it has been suggested that the relationship between damage size formed and G_{II} is so well defined that an instrumented drop weight test has been suggested as a method to measure G_{II}.[39]

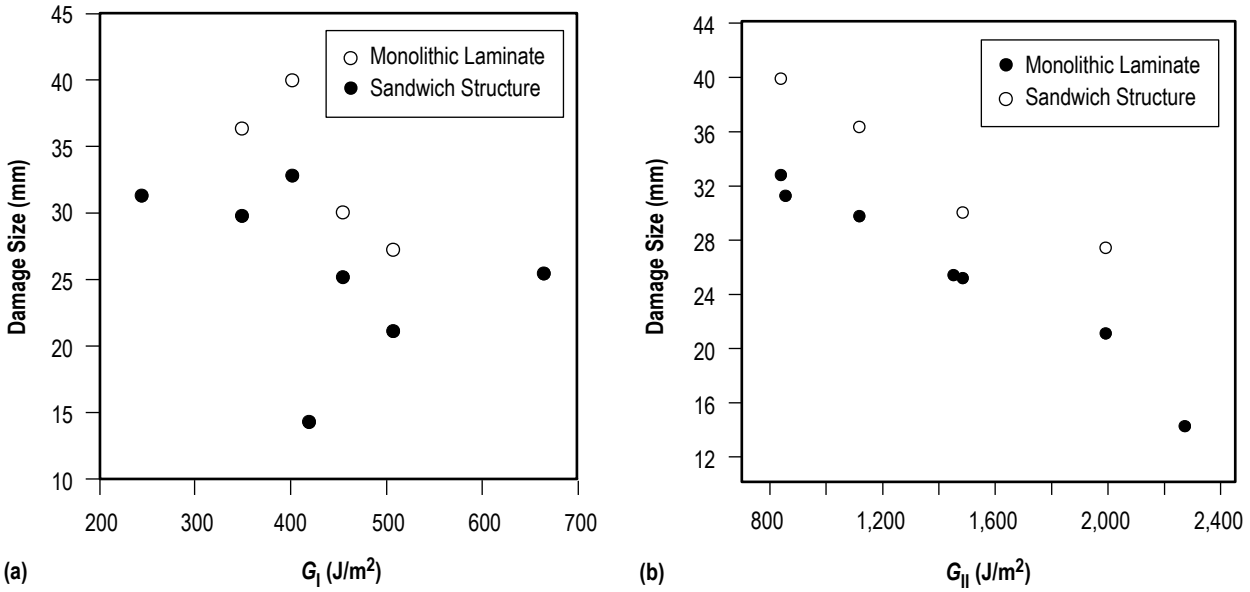

Figure 16. Damage size versus (a) G_{I} and (b) G_{II} .

Thus, increasing the mode I toughness has little to no effect on the damage tolerance of the laminates tested in this study. There is assumed to be some lower bound of which the mode I toughness would have an effect on CAI strength, as it is hard to envision a laminate with virtually no mode I toughness having the same damage tolerance as the laminates tested in this study. However, for the practical ranges of mode I toughness values typically encountered in structural applications, the magnitude of G_{I} appears to have little effect.

Since the impact damaged region of the laminate had sublaminate buckling occur (which has been noted by the author on most CAI specimens tested using digital image correlation and sometimes even seen with the unaided eye), the assumption is both that the buckled region cannot carry more load and any additional in-plane compressive load is now transferred around the buckled sublaminate. This causes stress concentrations on either side of the buckled laminate, just like a hole would cause stress redistribution around it. This being the case, at some applied stress, the load-bearing fibers at the edge of the damage zone that experience added loads due to the sublaminate buckling reach their ultimate stress value and microbuckle in the same fashion as laminates with holes. This is consistent with the observation that OHC strength is independent of mode I and mode II fracture toughness values.

With the data presented thus far, it is apparent that once damage is induced in a laminate, the mode I toughness value has no effect on the residual compression strength. However, since the residual strength is directly related to damage size, which in turn is directly related to mode II toughness, the effects of varying mode II toughness values on the residual compressive strength of a damaged laminate cannot be directly assessed. Because only one impact energy level was used and effects of changing mode II toughness values on residual strength may be attributed solely to damage size; i.e., if damage growth during a CAI test is governed by mode II toughness and not mode I toughness, as assumed in figure 2, then this cannot be ascertained with the data generated thus far.

As a check on the damage tolerance of laminates with similar size damage, but with differing G_I and G_{II} values, a limited series of CAI tests was performed comparing the CAI strength of resin systems 2 and 7 with equal size damage. It is recognized that although the damage sizes are equal, the through-thickness distribution of damage may not be, but if delamination growth is a driver, then lower CAI strength should still be seen for low toughness values despite small differences in damage morphology. In the first series of tests, resin system 2 was hit with about 22.4 J of impact energy to produce a damage size of about 33 mm. This was compared to CAI specimens of resin system 7 hit with 10.8 J of impact energy to produce a similar 33-mm damage size. A comparison of the NDE indications and cross sections through the damage zone are shown in figure 17.

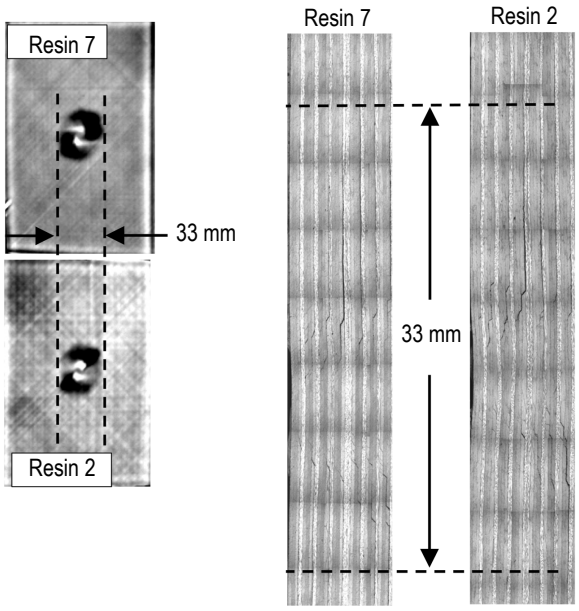

Figure 17. NDE indications and photomicrographs of cross sections for resin systems 2 and 7 with equal size damage (33 mm).

Subsequent CAI testing showed resin system 7 having a CAI strength of 269 ± 6 MPa and resin system 2 having a CAI strength of 284 ± 8 MPa. If G_{II} was a driver in the failure mechanism, the more than double value of G_{II} for resin system 2 should cause a notably higher CAI strength other than the measured 6% for the similar states of damage.

This type of test was repeated on the same two material systems using a smaller size damage. Resin system 2 was hit with 12.3 J and resin system 7 was hit with 5 J to create a damage size of about 23 cm in both. A comparison of the NDE indications and cross sections through the damage zone of these specimens with smaller damage are shown in figure 18.

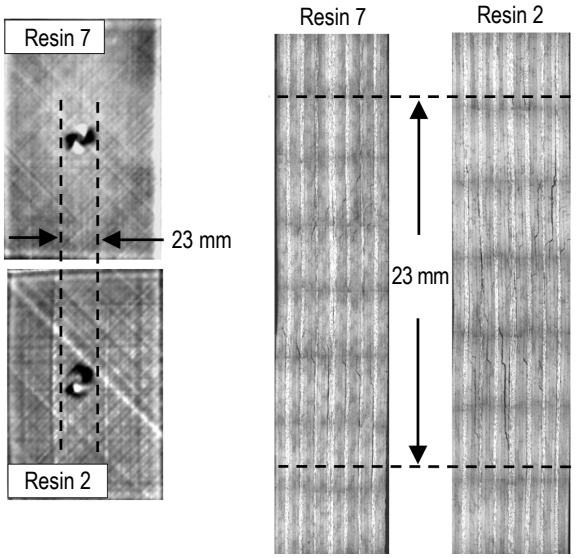

Figure 18. NDE indications and photomicrographs of cross sections for resin systems 2 and 7 with equal size damage (23 mm).

Subsequent CAI testing showed resin system 7 having a CAI strength of 373 ± 14 MPa and resin system 2 having a CAI strength of 346 ± 19 MPa. If G_{II} was a driver in the failure mechanism, the more than double value of G_{II} for resin system 2 should cause a notably higher CAI strength for the similar states of damage, but resin system 7 actually has the higher CAI strength. This is thought to be a result of less through-thickness damage to get a damage size of 23 mm in resin system 7, which supports the notion that damage formation is key to CAI strength, not delamination growth either by mode I or mode II during the subsequent in-plane compression event.

Even if delamination growth were present, at some point during the growth, the load not being carried by the new, bigger delamination would dump even more load on the 0° fibers at the edge of the damage zone. At some point, these fibers would be overloaded and fail by kink band formation. A recent paper[59] looked at these failure mechanisms analytically using finite element analysis and concluded that both delamination growth and/or fiber failure could occur depending on where (through the thickness) and how many artificial delaminations were inserted. The authors concluded that for most CAI cases, 'in-plane failure due to stress concentration is the dominant damage mechanism and delamination propagation is unlikely,' since many delaminations distributed through the thickness tend to occur. It should be noted that compression failure mechanisms due to foreign object debris (FOD) may differ from impact damage since FOD has one delamination and no microcracks, and impact damage typically contains numerous delaminations and microcracks.

6. CONCLUSIONS

Within the assumptions made in figures 1 and 2, the results of this study indicate that the mode I fracture toughness (as measured by the DCB test) have no effect on either the formation of damage due to impact or on the resulting residual compression strength of carbon/epoxy laminates, either as monolithic laminates or as face sheets of honeycomb sandwich structure. Thus, a delamination growth failure mechanism (that directly leads to failure) as assumed in figure 2 is not apparent in this study. The mode II fracture toughness (as measured by the ENF test) has a direct correlation on the size of the damage formed (verifying the assumption in fig. 1 and in ref. 39) and this size is what governs the CAI strength. The effects of mode II fracture toughness on any damage growth mechanisms during in-plane compressive loading also appeared to have no effect on the CAI strength of laminates with similar damage morphologies based on the limited tests performed in this study.

From the data in this study, it is apparent that the majority of damage tolerance of a quasi-isotropic laminate is attributed to its resistance to forming damage due to an impact event, and this damage formation is directly related to G_{II}. Once damage has developed, the CAI strength appears to be independent of G_I and G_{II}, and the equivalent hole model seems to describe CAI behavior well.

REFERENCES

1. Byers, B.A.: "Behavoir of damaged graphite/epoxy laminates under compression loading," NASA Contractor Report 159293, NASA Langley Research Center, Hampton, VA, August 1980.

2. Chai, H.; Babcock, C.D.; and Knauss, W.G.: "One dimensional modelling of failure in laminated plates by delamination buckling," *International Journal of Solids and Structures*, Vol. 17, pp. 1069–1083, <https://doi.org/10.1016/0020-7683(81)90014-7>, 1981.

3. Chai, H.; Knauss, W.G.; and Babcock, C.D.: "Observation of damage growth in compressively loaded laminates," *Experimental Mechanics*, Vol. 23, pp. 329–337, 1983.

4. Chai, H.; and Babcock, C.D.: "Two-dimensional modleling of compressive failure in delaminated laminates," *Journal of Composite Materials*, Vol. 19, pp. 67–98, 1985.

5. Suemasu, H.; Kumagai, T.; and Gozu, K.: "Compressive Behavior of Multiply Delaminated Composite Laminates Part 1: Experiment And Analytical Development," *AIAA Journal,* Vol. 36, No. 7, pp. 1279–1285, <http://dx.doi.org/10.2514/2.511>, 1998.

6. Gottesman, T.; Girshovich, S.; Drukker, E.; and Loy, J.: "Residual strength of impacted composites: Analysis and tests," *Journal of Composites Technology and Research*, Vol. 16, pp. 244–255, 1994.

7. Ishikawa, T.; Sugimuto, S.; Matsushima, M.; and Hayashi, Y.: "Some experimental findings in compression-after-impact (CAI) tests of CF/PEEK (APC-2) and conventional CF/epoxy flat plates," *Composites Science and Technology*, Vol. 55, No. 4, pp. 349–363, 1995.

8. de Freitas, M.; and Reis, L.: "Failure mechanisms on composites specimens subjected to compression after impact," *Composite Structures*, Vol. 42, No. 4, pp. 365–373, <https://doi.org/10.1016/S0263-8223(98)00081-6>, August 1998.

9. Greenhalgh, E.; and Singh, S.: "Investigation of the failure mechanisms for delamination growth from embedded defects," *Proceedings ICCM 12*, Paris, July 5–9, 1999.

10. Short, G.J.; Guild, F.J.; and Pavier, M.J.: "The effect of delamination geometry on the compressive failure of composite laminates," *Composites Science and Technology 2001*, Vol. 61, pp. 2075–2086, 2001.

11. Jones, R.; Baker, A.A.; and Callinan, R.J.: "Residual strength of impact damaged composites," *Composite Structures*, Vol. 2, pp. 371–372, 1984.

12. Aoki, Y.; Kondo, H.; and Hatta, H.: "Effect of delamination propagation on mechanical behavior in compression after impact," *Proceedings 16th International Conference on Composite Materials*, Kyoto, Japan, July 8–13, 2007.

13. Subramanian, A.; Dayal, V.; and Barnard, D.J.: "Damage characterization of carbon/epoxy laminates using compression-after-impact (CAI) and ultrasonic NDE," *American Institute of Physics Conference Proceedings 1511*, Ames, IA, July 1, 2012.

14. Rhead, A.T.; and Butler, R.: "Compression static strength model for impact damaged laminates," *Composites Science and Technology*, Vol. 69, pp. 2301–2307, 2009.

15. Harman, A.; Litchfield, A.; and Thomson, R.: "Preliminary review of physically based methodologies for predicting the strength of visibly damaged composite laminates," *Materials Science Forum*, Vol. 654, pp. 654–656, 2587–2591, 2010.

16. Shivakumar, K.N.; and Whitcomb, J.D.: "Buckling of a sublaminate in a quasi-isotropic composite laminate," NASA Technical Memorandum 85755, NASA Langley Research Center, Hampton, VA, 1984.

17. Finn, S.R.; and Springer, G.S.: "Compressive strength of damaged and repaired composite plates, "*Proceedings of the 9th DOD/NASA/FAA conference on fibrous composites in structural design*," pp. 1083–1095, Lake Tahoe, NV, November 4–7, 1991.

18. Butler, R.; Rhead, A.T.; Liu, W.; and Kontis, N.: "Compressive strength of delaminated aerospace composites," *Philosophical Transactions of the Royal Society of London, Series A,* Vol. 370, pp. 1759–1779, 2012.

19. Xie, D.; and Biggers, S.B.: "Delamination growth and residual strength of compressively loaded sandwich panels with stiffness tailored face sheets," *Journal of Sandwich Structures and Materials*, Vol. 11, pp. 133–150, 2009.

20. Zhou, G.; and Rivera, L.A.: "Investigation for the reduction of in-plane compressive strength in preconditioned thin composite panels," *Journal of Composite Materials*, Vol. 39, pp. 391–421, 2005.

21. Rhead, A.T.; Butler, R.; and Baker, N.: "Analysis and compression testing of laminates optimized for damage tolerance," *Applied Composite Materials*, Vol. 18, pp. 85–100, 2011.

22. Woodward, M.R.; Owens, S.D.; LAW, G.E.; and Mignery, L.A.: "Applications of damage tolerance analysis methodology in aircraft design and production," General Dynamics Technical Paper 1991, pp. 1071–1081 (available as nasa_techdoc_19950022062), 2011.

23. Yan, H.Y.; Oskay, C.; Krishnan, A.; and Xu, L.R.: "Compression-after-impact response of woven fiber-reinforced composites," *Composites Science and Technology*, Vol. 70, pp. 2128–2136, 2010.

24. Ireman, T.; Thesken, J.C.; Greenhalgh, E.; et al.: "Damage propagation in composite structural elements-coupon experiments and analyses," *Composite Structures*, Vol. 36, pp. 209–220, 1996.

25. Fink, B.K.; Monib, A.M.; and Gillespie, J.W.: "Damage tolerance of thick-section composites subjected to ballistic impact," ARL-TR-2477, May 2001.

26. Suemasu, H.; Sasaki, W.; Ishikawa, T.; and Aoki, Y.A.: "A numerical study on compressive behavior of composite plates with multiple circular delaminations considering delamination propagation," *Composites Science and Technology*, Vol. 111, pp. 147–157, 2014.

27. De Moura, M.; Goncalves, J.; Marques, A.; and DeCastro, P.: "Modelling compression failure after low velocity impact on laminated composites using interface elements," *Journal of Composite Materials*, Vol. 31, pp. 1462–1479, 1997.

28. Kinawy, M.; and Butler, R.: "Face damage growth of sandwich composites under compressive loading," *Proceedings ICCM 17*, Edinburgh, U.K., July 27–31, 2009.

29. Reeder, J.R.; Chunchu, P.B.; Song, K.; and Ambur, D.R.: "Postbuckling and growth of delaminations in composite plates subjected to axial compression," AIAA Paper 2002-1746, 43rd AIAA/ASME/ASCE/AHS/ASC Structures, Structural Dynamics, and Materials Conference, Denver, CO, April 22–25, 2002.

30. Masters, J.E.: "Improved impact and delamination resistance through interleafing," *Key Engineering Materials*, Vol. 37, pp. 317–348, 1989.

31. Recker, H.G.; Altstadt, V.; Eberle, W.; et al.: "Toughened thermosets for damage tolerant carbon fiber reinforced composites," *SAMPE Journal*, Vol. 26, No. 2, pp. 73–78, 1990.

32. Kuwata, M.: "Mechanisms of interlaminar fracture toughness using non-woven veils as interleaf materials," Ph.D. Thesis, Queen Mary, University of London, 2010.

33. Poe, C.C.; Portanova, M.A.; Masters, J.E.; et al.: "Comparison of impact results for several polymeric composites over a wide range of low impact velocities," NASA Conference Publication 3104, NASA Langley Research Center, Hampton, VA, 1993.

34. Prichard, J.C.; and Hogg, P.J.: "The role of impact damage in post-impact compression testing," *Composites*, Vol. 21, pp. 503–511, 1990.

35. Ghasemi Nejhad, M.N.; and Parvizi-Majidi, A.: "Impact behavior and damage tolerance of woven carbon fibre-reinforced thermoplastic composites," *Composites*, Vol. 21, pp. 155–168, 1990.

36. Dempsey, R.L.; and Horton, R.E.: "Damage tolerance evaluation of several elevated temperature graphite composite materials," *Proceedings 35th International SAMPE Symposium*, pp. 1292–1305, April 2–5, 1990.

37. Cantwell, W.J.; Curtis, P.T.; and Morton, J.: "An assessment of the impact performance of CFRP reinforced with high-strain carbon fibres," *Composites Science and Technology*, Vol. 25, pp. 133–148, 1986.

38. Dow, M.B.; and Smith, D.L.: "Properties of two composite materials made of toughened epoxy resin and high-strain graphite Fiber," NASA Technical Paper 2826, NASA Langley Research Center, Hampton, VA, July 1988.

39. Cartie, D.D.R.; and Irving, P.E.: "Effect of resin and fibre properties on impact and compression after impact performance of CFRP, *Composites: Part A*, Vol. 33, pp. 483–493, 2002.

40. Hodge, A.J.; Nettles, A.T.; and Jackson, J.R.: "Comparison of open-hole compression strength and compression after impact strength on carbon fiber/epoxy laminates for the ASRES I composite interstage," NASA Technical Paper 216460, NASA Marshall Space Flight Center, Huntsville, AL, 2011.

41. Soutis, C.; Smith, F.A.; and Matthews, F.L.: "Predicting the compressive engineering performance of carbon fiber-reinforced plastics," *Composites*: *Part A*, Vol. 31, pp. 531–536, 2000.

42. Guild, F.J.; Hogg, P.J.; and Prichard, J.C.: "A model for the reduction in compression strength of continuous fiber composites after impact damage," *Composites*, Vol. 24, No. 4, pp. 333–339, 1993.

43. Soutis, C.; and Curtis, P.T.: "Prediction of the post-impact compressive vstrength of CFRP laminated composites," *Composites Science and Technology*, Vol. 56, pp. 677–684, 1996.

44. Puhul, C.; Zhen, S.; and Jun Yang, W.: "A new method for compression after impact strength prediction of composite laminates," *Journal of Composite Materials*, Vol. 36, pp. 589–610, 2002.

45. Bull, D.J.; Spearing, S.M.; and Sinclair, I.: "Quasi-static indentation and compression after impact damage growth monitoring using microfocus X-Ray computed tomography," *Proceedings 19th International Conference on Composite Materials*, Montreal, Canada, July 28–August 2, 2013.

46. Revallant, S.; Bouvet, C.; Abi Abdallah, E.; et al.: "Experimental analysis of CFRP laminates subjected to compression after impact: The role of impact-induced cracks in failure," *Composite Structures*, Vol. 111, pp. 147–157, 2014.

47. Edgren, F.; Asp, L.E.; and Bull, P.H.: "Compressive failure of impacted NCF composite sandwich panels—Characterization of the failure process," *Journal of Composite Materials*, Vol. 38, pp. 495–514, 2004.

48. Czabaj, M.W.; Zehnder, A.T.; Davidson, B.D.; and Singh, A.K.; "Compressive strength of honeycomb-stiffened graphite/epoxy sandwich panels with barely-visible indentation damage," *Journal of Composite Materials*, Vol. 48, pp. 2455–2471, 2014.

49. Edgren, F.; Soutis, C.; and Asp, L.E.: "Damage tolerance analysis of NCF composite sandwich panels," *Composites Science and Technology*, Vol. 68, pp. 2635–2645, 2008.

50. Edgren, F.: "Compressive failure of NCF composites," *Proceedings 20th Technical Conference of the American Society for Composites*, Paper No. 26, Philadelphia, PA, September 7–9, 2005.

51. Lee, J.; Soutis, C.; and Kong, C.: "Prediction of compression-after-impact (CAI) Strength of CFRP Laminated Composites," *Proceedings 18th International Conference on Composite Materials*, Jeju, Korea, August 21–26 2011.

52. Portanova, M.A.: "Evaluation of the impact response of textile composites," NASA Contractor Report 198265, NASA Langley Research Center, Hampton, VA, 1995.

53. Bull, D.J.; Spearing, S.M.; and Sinclair, I.: "Observations of damage development from compression-after-impact experiments using ex situ micro-focus computed tomography," *Composites Science and Technology*, Vol. 97, pp. 106–114, 2014.

54. O'Brien, T.K.; Johnston, W.M.; and Toland, G.J.: "Mode II interlaminar fracture toughness and fatigue characterization of a graphite epoxy composite material," NASA Technical Memorandum 2010-216838, NASA Marshall Space Flight Center, Huntsville, AL, August 2010.

55. Standard Test Method for Mode I Interlaminar Fracture Toughness of Unidirectional Fiber-Reinforced Polymer Matrix Composites, ASTM Standard D5528-01, American Society for Testing and Materials Annual Book of Standards, Vol. 15.03, pp. 284–295, 2013.

56. Standard Test Method for Open-Hole Compressive Strength of Polymer Matrix Composite Laminates, ASTM Standard D6484-09, American Society for Testing and Materials Annual Book of Standards, Vol. 15.03, pp. 392–407, 2013.

57. Standard Test Method for Compressive Residual Strength Properties of Damaged Polymer Matrix Composite Laminates, ASTM Standard D7137-12, American Society for Testing and Materials Annual Book of Standards, Vol. 15.03, pp. 513–529, 2013.

58. Nettles, A.T.; and Jackson, J.R.: "Developing a material strength design value based on compression after impact damage for the ARES I composite interstage," NASA/TP—2009–215634, NASA Marshall Space Flight Center, Huntsville, AL, 2009.

59. Yang, Y.; and Li, S.: "CAI damage mechanism characterization," *Proceedings 20th International Conference on Composite Materials*, Copenhagen, Denmark, July 19–24, 2015.

REPORT DOCUMENTATION PAGE

Form Approved
OMB No. 0704-0188

The public reporting burden for this collection of information is estimated to average 1 hour per response, including the time for reviewing instructions, searching existing data sources, gathering and maintaining the data needed, and completing and reviewing the collection of information. Send comments regarding this burden estimate or any other aspect of this collection of information, including suggestions for reducing this burden, to Department of Defense, Washington Headquarters Services, Directorate for Information Operation and Reports (0704-0188), 1215 Jefferson Davis Highway, Suite 1204, Arlington, VA 22202-4302. Respondents should be aware that notwithstanding any other provision of law, no person shall be subject to any penalty for failing to comply with a collection of information if it does not display a currently valid OMB control number.
PLEASE DO NOT RETURN YOUR FORM TO THE ABOVE ADDRESS.

1. REPORT DATE *(DD-MM-YYYY)*	2. REPORT TYPE	3. DATES COVERED *(From - To)*
01–07–2017	Technical Publication	

4. TITLE AND SUBTITLE

The Influence of G_I and G_{II} on the Compression After Impact Strength of Carbon Fiber/Epoxy Laminates and Sandwich Structure

5a. CONTRACT NUMBER

5b. GRANT NUMBER

5c. PROGRAM ELEMENT NUMBER

6. AUTHOR(S)

A.T. Nettles and L.L. Scharber

5d. PROJECT NUMBER

5e. TASK NUMBER

5f. WORK UNIT NUMBER

7. PERFORMING ORGANIZATION NAME(S) AND ADDRESS(ES)

George C. Marshall Space Flight Center
Huntsville, AL 35812

8. PERFORMING ORGANIZATION REPORT NUMBER

M–1437

9. SPONSORING/MONITORING AGENCY NAME(S) AND ADDRESS(ES)

National Aeronautics and Space Administration
Washington, DC 20546–0001

10. SPONSORING/MONITOR'S ACRONYM(S)

NASA

11. SPONSORING/MONITORING REPORT NUMBER

NASA/TP—2017–219635

12. DISTRIBUTION/AVAILABILITY STATEMENT

Unclassified-Unlimited
Subject Category 24
Availability: NASA STI Information Desk (757–864–9658)

13. SUPPLEMENTARY NOTES

Prepared by the Materials and Processes Laboratory, Engineering Directorate

14. ABSTRACT

This study measured the compression after impact strength of IM7 carbon fiber laminates made from epoxy resins with various mode I and mode II toughness values to observe the effects of these toughness values on the resistance to damage formation and subsequent residual compression strength-carrying capabilities. Both monolithic laminates and sandwich structure were evaluated. A total of seven different epoxy resin systems were used ranging in approximate G_I values of 245–665 J/m^2 and approximate G_{II} values of 840–2275 J/m^2. The results for resistance to impact damage formation showed that there was a direct correlation between G_{II} and the planar size of damage, as measured by thermography. Subsequent residual compression strength testing suggested that G_I had no influence on the measured values and most of the difference in compression strength was directly related to the size of damage. Thus, delamination growth assumed as an opening type of failure mechanism does not appear to be responsible for loss of compression strength in the specimens examined in this study.

15. SUBJECT TERMS

delamination growth, damage tolerance, impact damage, failure mechanisms, kink band formation

16. SECURITY CLASSIFICATION OF:			17. LIMITATION OF ABSTRACT	18. NUMBER OF PAGES	19a. NAME OF RESPONSIBLE PERSON
a. REPORT	b. ABSTRACT	c. THIS PAGE			STI Help Desk at email: help@sti.nasa.gov
U	U	U	UU	40	19b. TELEPHONE NUMBER *(Include area code)*
					STI Help Desk at: 757–864–9658

National Aeronautics and
Space Administration
IS02
George C. Marshall Space Flight Center
Huntsville, Alabama 35812